Characterization of Lithium-6 as a Commercial Helium-3 Alternative for Nuclear Safeguards and Security

A Thesis Presented for the
Master of Science
Degree
The University of Tennessee, Knoxville

Alexander Martin Okowita
December 2014

ACKNOWLEDGEMENTS

I am very grateful for the assistance and guidance Dr. Alex Enders and Dr. Jason Hayward have provided on this project. Their in-depth knowledge and practical experience have been invaluable towards my work and to my development as an aspiring researcher. I would like to extend my appreciation to my committee members, Dr. Skutnik and Dr. Lukosi for their efforts, suggestions, and challenging questions. I would also like to thank the many people at Oak Ridge National Laboratory that helped with various aspects this project: Steve Cleveland for always being available to babysit me in the Lab, Shaheen Dewji for her incredible advice and editing prowess, Jeff Chapman and Louise Evans for the references and papers they provided, Steven Croft and Bob McElroy for their incredibly in-depth knowledge, Jim Younkin for his electrical wiring expertise, and Ian Gross for his assistance in anything and everything I needed. I would like to extend my upmost gratitude to my loving parents Ted and Linda, as well as my sister Lindsay. Lastly I would like to thank my wife Samantha for her constant patience, encouragement, and unconditional love, and without whom this contribution would not be possible.

ABSTRACT

Helium-3 detectors are efficient, reliable neutron detectors, but their high demand has reduced their supply to a very miniscule level, making them very expensive. The goal of this project is to test and evaluate an alternative produced by industry. Current testing is being done with a Lithium Zinc Sulfide (^{6}LiF:ZnS(Ag)) detector from Aspect used in their portal monitors.

There are three basic requirements for neutron detectors used in nuclear safeguards and security: 1) high absolute detection efficiency, 2) maintaining neutron detection efficiency when simultaneously exposed to a high gamma ray exposure rate, and 3) the ability to maintain neutron detection rate in all operational temperature ranges. All of these requirements will be tested with the detector mentioned above, including comparisons to a helium-3 slab counter from Rapiscan. This thesis describes the results of said detector systems, which were tested at Oak Ridge National Laboratory.

TABLE OF CONTENTS

I. Introduction 1

A. Criteria to be Evaluated for Alternative ^{3}He 2

B. Efficiency Considerations 5

C. Example Technologies 7

1) BF_3 Filled Proportional Counters 7

2) Boron Lined Straw Counters 7

3) Lithium-6 Loaded Glass Fibers 8

4) Lithium Coated Zinc Sulfide Scintillator 8

D. Previous Testing 8

E. Systems Being Tested 9

II. Experimental Methods and Procedure 13

A. Test 1: Absolute Neutron Detection Efficiency and Radial Response 14

B. Test 2: Gamma Absolute Rejection Ratio for Neutrons 14

C. Test 3: Moderation Response 15

D. Test 4: Environmental Testing 17

III. Results and Discussion 20

A. Test 1: Absolute Neutron Detection Efficiency and Radial Response 20

B. Test 2: Gamma Absolute Rejection Ratio for Neutrons 22

C. Test 3: Moderation Response 24

D. Test 4: Environmental Testing 25

IV. MCNP Modeling 32

V. Conclusions and Future Work 36

A. Conclusions 36

B. Suggested Future Work 36

Bibliography 38

Appendices 41

Appendix A: Other Detectors Analyzed 42

Boron Coated Straw 42

Appendix B: Tabular Data from Plots 44

Test 1: Absolute Neutron Detection eEficiency and Radial Response 44

Test 2: Gamma Absolute Rejection Ratio for Neutrons 44

Test 3: Moderation Response 45

Test 4: Environmental Testing 45

Appendix C: MCNP Input Files 46

Helium-3 Profile Base Input 46

Lithium-6 Profile Base Input 47

Helium-3 Efficiency Input 48

Lithium-6 Efficiency Input 49

Vita 51

LIST OF TABLES

Table 1 – Requirements for replacement Helium-3 detectors [4] 3

Table 2 – Thermal absorption cross sections for nuclide reactions 6

Table 3 – Results reported from PNNL studies of prototype replacement technologies [5] 9

Table 4 – Measured absolute neutron detection efficiency for both neutron modules 22

Table 5 – Gamma Absolute Rejection Ratio for neutrons for both modules 24

Table 6 – Comparison of the absolute neutron detection efficiency as taken from experimental results and from Monte Carlo analysis 32

Table 7 – Table outlining the requirements and experimental data for neutron efficiency and GARRn 36

Table 8 – Neutron profile data 44

Table 9 – Neutron response to a gamma source data 44

Table 10 – Moderation response data 45

Table 11 – Environmental testing data 45

LIST OF FIGURES

Figure 1 – Absorption cross sections for replacement technologies [2] 5

Figure 2 – Li:ZnS(Ag) detector from Aspect 10

Figure 3 – TSA Helium-3 module with front cover of moderator box removed 12

Figure 4 – Testing Cart with mounted Lithium-6 (left) and Helium-3 (right) modules 13

Figure 5 – Illustration of the source progression during the first part of test one 14

Figure 6 – Photo of the gamma source on a stand in front of the Lithium-6 module 15

Figure 7 – Nested polyethylene spheres for testing 16

Figure 8 – Photos of the spheres setup for testing: Californium source (left), smallest sphere (center), and largest sphere (right) 16

Figure 9 – Photo of the source stand inside the environmental testing chamber 18

Figure 10 – Helium-3 (left) and Lithium-6 (right) modules setup in the test chamber 19

Figure 11 - Plot of the mean neutron count rate as a source is moved laterally across the face of the detectors where zero is directly in front of the detectors. 21

Figure 12 - Mean neutron count rate response of each detector as a gamma source is moved closer to the detector face 22

Figure 13 – Zooming in from Figure 12, the mean count rate response of the Lithium-6 module is shown as the gamma source is moved closer to the detector face with error included. The bounds shown in red as outlined in [4] are within 10% of the mean count rate response with no gamma source present 23

Figure 14 - Zooming in from Figure 12, the mean count rate response of the Lithium-6 module is shown as the gamma source is moved closer to the detector face. The bounds shown in red as outlined in [4] are within 10% of the mean count rate response with no gamma source present 24

Figure 15 - Neutron response for each module to the addition of increasing thicknesses of polyethylene 25
Figure 16 - Mean neutron count rate response for both modules to a change in temperature 27
Figure 17 – Mean neutron count rate response for the Lithium-6 module to changing temperature 28
Figure 18 - Mean neutron count rate response for the Helium-3 module to changing temperature 29
Figure 19 - Figure of Merit for all temperature measurements taken 30
Figure 20 – Plot showing the increase in dark current in a PMT as temperature increases. [14]. 31
Figure 21 - Comparison between experimental and simulated mean neutron count rate profiles for the Lithium-6 module 33
Figure 22 - Comparison between experimental and simulated mean neutron count rate profiles for the Helium-3 module 34
Figure 23 – MCNP simulation of the mean neutron count rate for an increasing thickness of polyethylene moderator face plate on the Helium-3 Module. 35
Figure 24 – Stopping power equivalence between straw detectors (4mm diameter) lined with 1 μm of $^{10}B_4C$, and ^{3}He gas. [10] 42
Figure 25 – Photo of the electronics and BCS detector all contained within a Pelican case 43
Figure 26 – Full testing setup with the Boron-10 (left), Lithium-6 (center), and Helium-3 (right) modules 43

I. INTRODUCTION

Thermal neutron detectors are used in a variety of different fields ranging from nuclear physics for homeland security to oil well logging. The material of choice for the development of thermal neutron detectors is currently helium-3 (^{3}He). ^{3}He is used in some of the Radiation Portal Monitors (RPMs) which have been placed all over the world by various government and commercial entities at sea ports and border crossings to detect the illicit smuggling of radiological and special nuclear materials (SNM) into the United States. ^{3}He is also used in nuclear safeguards by many international organizations such as the International Atomic Energy Agency (IAEA) for the quantification of SNM at various nuclear facilities around the world. Most of the ^{3}He supply in the United States comes from the Savannah River Site from the decay of tritium used in nuclear weapons development. The events of September 11th 2001 served to greatly accelerate the deployment of RPMs around the world. This massive increase in the demand of ^{3}He has diminished the stockpile and created an alarming shortage of the material. U.S. Government agencies have responded to this shortage by developing, and funding, programs to identify and implement replacement technologies for ^{3}He. [1]

This project specifically focused on RPMs, which are designed to detect the presence of gamma rays and neutrons produced by uranium and plutonium (^{235}U and ^{238}Pu specifically), each of these being key components in nuclear weapons. Around 64,000 containers and over one million people are screened daily by DHS, requiring a very low occurrence of false alarms in RPMs. Additionally, RPMs also must be able to detect the presence of SNM within a certain degree of accuracy [2]. This presents a problem in their development because a nefarious actor may have the foresight to shield their stolen SNM, which detracts from the radiation signal seen

by the detectors. This is compounded further by the fact there are many non-threatening sources of radioactivity such as spurious changes in background radiation, radioactive sources in building materials, and radiopharmaceuticals that lead to a large number of false alarms seen every day.

RPMs typically use both gamma and neutron detectors in their modules to maximize the probability of detecting illicit nuclear material. Because gamma rays are produced by all forms of radioactive materials, the main component of all RPMs is the gamma detection portion. For gamma detection, RPMs use a material called polyvinyl toluene (PVT) which is a very well understood technology. PVT is extremely cheap to manufacture, and is readily available. Although gamma detectors are the primary component, RPMs also employ a neutron detection portion for sensing plutonium, which emits significant levels of neutron radiation. Since shielding SNM from gamma rays requires heavy elements, and shielding from neutron requires light elements, having both detectors present on the RPM maximizes the probability of detection [3].

The development of alternative ^{3}He technologies has been in progress for many years, which has produced a great deal of both theorizing and testing to determine suitable replacement materials. Several prototypes have been developed and tested, and this work investigates a particular alternative thermal neutron detector that does not use ^{3}He.

A. Criteria to be Evaluated for Alternative ^{3}He

The isotope ^{3}He is considered the best option for neutron detectors. It has a high cross section for thermal neutrons, and its sensitivity to gamma rays is almost negligible. The Department of Homeland Security (DHS) has established strict requirements that must be met to ensure all replacements maintain similar standards. [4]. Prototyping has already demonstrated for our test system that many of these requirements have already been met. [5, 6], The performance criteria deemed most important are absolute neutron detection efficiency, intrinsic gamma-neutron

efficiency (or, the fraction of gammas misclassified as neutrons), gamma absolute rejection ratio for neutrons (GARRn), and temperature response of the detector. Table 1 describes the requirements outlined in [4] for RPMs.

Table 1 – Requirements for replacement Helium-3 detectors [4]

Parameter	*Specification*
Absolute neutron detection efficiency (at 2m)	$\varepsilon_{abs\ n} \geq 1.2x10^{-5}$ (2.5 cps/ng of ^{252}Cf)
Intrinsic gamma-neutron detection efficiency	$\varepsilon_{int\ \gamma,\ n} \leq 10^{-6}$ at 10 mR/hr
Gamma absolute rejection ratio for neutrons (GARRn)	$0.9 \leq GARRn \leq 1.1$ at 10 mR/hr
Operational temperature range	$-40^{o}C \leq$ Operational Temperature $\leq 55^{o}C$
Cost	At most $30,000 per RPM system

Absolute neutron detection efficiency is a measure of the fraction of neutrons emitted per ng from a bare ^{252}Cf source that are detected by the detector for a source-detector separation of 2m, this is shown in Equation 1.

$$\varepsilon_{absn} = \frac{\left(Number\ of\ \ pulses\ recorded\right)}{Number\ of\ \ neutron\ emitted\ \ from\ source} \tag{1}$$

Since the specific neutron emission rate of ^{252}Cf per ng is well known (2.314 x 10^6 neutrons/sec/microgram [15]), the reported absolute efficiency measurements are in units of counts per second per ng of ^{252}Cf located within the bare source. DHS specifies that an acceptable ^{3}He replacement should have an absolute neutron detection efficiency of at least 2.5 cps/ng ^{252}Cf when a source is placed two meters away from the center of the front face of the detector. The intrinsic gamma-neutron detection efficiency ($\varepsilon_{int\ \gamma,\ n}$) is the fraction of gamma rays incident upon the detector surface that are mistakenly recorded as neutrons. Free neutrons have a characteristic half-life of 10.6 minutes, [16] so the vast majority of free neutrons that are generated by cosmic events decay before reaching Earth and are thus not commonly present in background radiation at terrestrial elevations. Neutrons are also not commonly emitted by either construction materials or radiopharmaceuticals. Since there are few legitimate background

sources of ambient neutrons, every neutron alarm from an RPM must be taken very seriously. Conversely, there are many legitimate sources of ambient gamma ray producers such as medical procedures and innocuous consumer goods; therefore, neutron detectors that respond to gamma rays are undesirable for use in RPMs. DHS has set a threshold for gamma sensitivity at 10^{-6}, or less than one count in a million. The 10 mR/hr field is the number of gamma rays incident on the detector surface per hour, the calculation of this metric is outlined in Equation 2 [22].

$$\frac{mR}{hr} = \frac{6CEf}{d^2} \tag{2}$$

where:
C = activity (mCi)
E = Gamma Ray Energy (MeV)
f = fraction of decays yielding gamma
d = distance from the source (ft)

The GARRn is the absolute neutron detection efficiency in the presence of a strong gamma source over the absolute neutron detection efficiency with no gamma source present. The calculation is outlined in Equation 3.

$$GARRn = \frac{\varepsilon_{abs\gamma,n}}{\varepsilon_{absn}} \tag{3}$$

This measure of a detector determines how the detector will react in the presence of large gamma sources. Because a nefarious actor could hide a neutron source within a container of innocuous substances such as radiopharmaceuticals, it is important for the detector to still recognize a neutron signature, and should not deviate from a normal count by more than 10% in either direction when exposed to a high gamma ray field.

B. Efficiency Considerations

Of all of the alternatives researched early on, both ^{10}B and ^{6}Li show promise as ^{3}He replacements. They both have high capture cross sections, good neutron detection efficiency, and detectors made from these isotopes are also relatively insensitive to gamma rays. The efficiency of neutron detectors is a function of the neutron moderator design and the thermal-neutron capture reaction with isotopes such as ^{3}He, ^{10}B, and ^{6}Li. Figure 1 shows the reaction cross-sections for the replacement isotopes mentioned previously. Considering thermal energy, ^{3}He has the largest cross section, but ^{10}B is only about 30% lower, while the ^{6}Li thermal-neutron cross section is about a factor of 6 lower than ^{3}He.

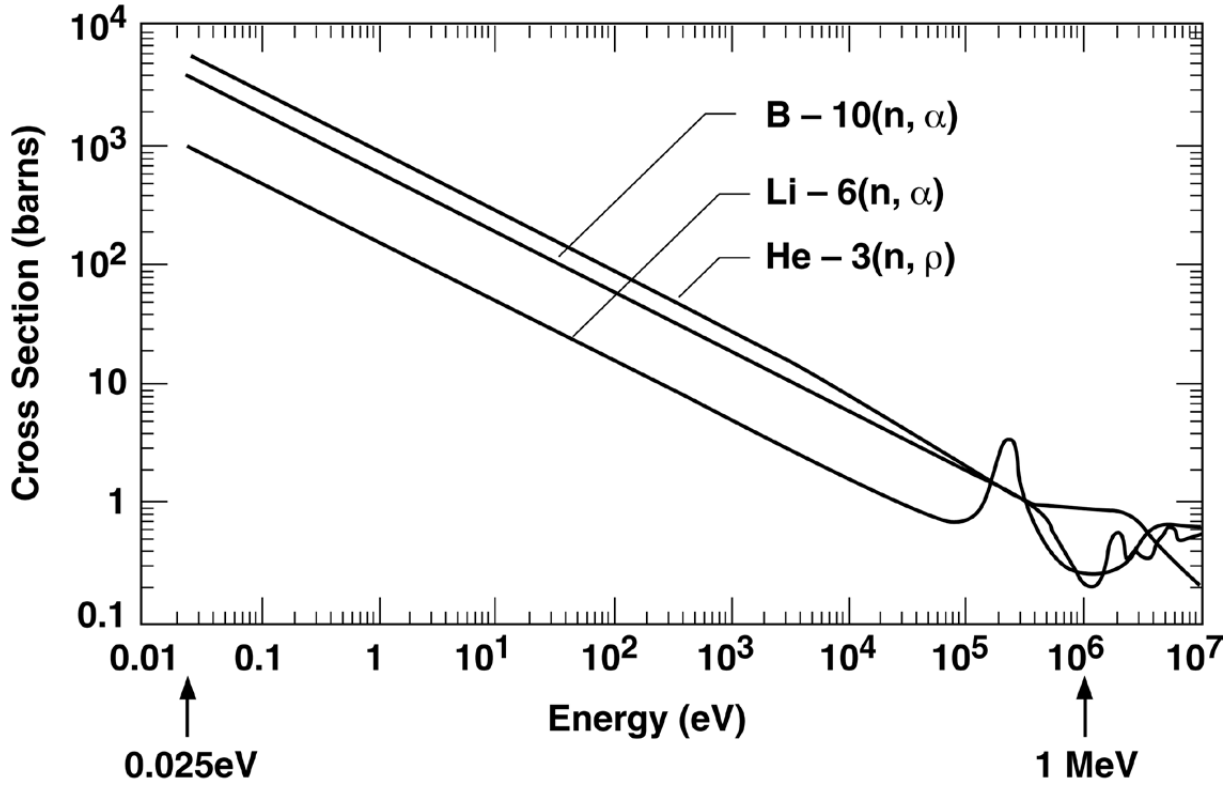


Figure 1 – Absorption cross sections for replacement technologies [2]

Table 2 – Thermal absorption cross sections for nuclide reactions

Nuclide	*Reaction*	*Absorption Cross Section*
^{3}He	^{3}He(n,p)α	5333 b
^{6}Li	^{6}Li(n,α)^{3}H	940 b
^{10}B	^{10}B(n,^{7}Li)α	3835 b

Most of the neutron sources of interest for safeguards come from spontaneous fission, induced fission, and (α, n) reactions. The average energy of these neutrons is typically within the range of 1-2 MeV, forcing the need to moderate the neutrons, slowing them down enough to be absorbed by the detection medium [7]. Hydrogen is the most efficient at reducing the energy of fast neutrons, so typically high density polyethylene (HDPE) is used for moderation. The isotopes ^{10}B and ^{7}Li can exist in solid forms, and as the atom density is much higher for a solid then a gas, less moderating material is needed.

The two most common ways of detecting thermal neutrons are proportional detectors and scintillators. In both of these methods a thermal neutron is captured by the detection isotope used which then emits charged particles. The first method of detection takes advantage of the resulting ionizations to "count" the number of neutron interactions. To employ this method, a bias is applied across the detection medium; this bias causes a charge to be carried through the electrode when neutron capture occurs, and through subsequent ionizations. When the charge reaches the electrode, a count is registered. In the second method, the charged particles cause ionization that, in turn, emits visible light on their relaxation. This light can be collected by a light collection device such as a photomultiplier tube (PMT) which amplifies the light so that it can be measured as a count. Scintillators are typically made from liquids and solids, and are, therefore, generally more sensitive to gamma rays compared with gasses.

C. Example Technologies

Neutron detection technology development is an active area of research and a number of novel technologies and devices are currently being investigated [3]. Of the available neutron detection technologies, there are two main isotopes that are potential candidates for replacing ^{3}He: ^{10}B and ^{6}Li. Boron counters are considered proportional counters (like ^{3}He) and are either in the form of boron trifluoride (BF_3) gas or boron lined proportional straws [2, 10, 11]. Gas proportional counters are relatively insensitive to gamma-ray interactions as compared to solids and liquids due to the low average density of gases. Lithium counters are scintillators, so they require a photomultiplier tube (PMT) for measurement; this technology is formulated either in scintillating glass fibers or lithium coated zinc sulfide scintillators [13].

1) BF_3 Filled Proportional Counters

This technology is essentially a drop-in replacement for current ^{3}He tubes. They have equivalent gamma insensitivity compared with ^{3}He tubes, but have much lower neutron sensitivity [2, 9]. This lower sensitivity is caused by the lower capture cross-section and pressure limitations of BF_3 due to its hazardous nature. Because it is a hazardous gas, it is subject to strict US Department of Transportation regulations. This would cause the replacement process to be long, expensive, and tedious, if it were allowed at all, which is the major concern for using BF_3 as a replacement.

2) Boron Lined Straw Counters

Boron lined straws are a direct replacement for current ^{3}He tubes. They have lower neutron sensitivity than ^{3}He tubes because the neutron absorber (^{10}B) is on the walls of the tube rather than occupying the entire volume. However, they do not contain hazardous materials, they have similar gamma insensitivity to ^{3}He tubes [9], and the

lower cross section for absorption can be countered by utilizing more tubes. The current approach is to pack hundreds of tiny tubes into an array that can mimic the response from a ^{3}He tube where a similar efficiency can be reached in the same volume.

3) Lithium-6 Loaded Glass Fibers

This technology is ^{6}Li-enriched lithium silicate glass fibers doped with ^{3+}Ce. The composition of the glass is 57% SiO_2, 17% $^{6}Li_2O$ (enriched to 95% ^{6}Li), 18% Al_2O_3, 4% MgO and 4% Ce_2O_3 [17]. The material is formed into a uniform glass composite with the percentages above and then used as a scintillator. These fibers do not currently meet the absolute neutron detection efficiency outlined in [4]. [5] The use of PMTs in the scintillators also adds additional environmental stability requirements.

4) Lithium Coated Zinc Sulfide Scintillator

This technology has good neutron sensitivity and fair neutron-gamma separation and is currently the most likely option for alternative neutron detectors. Silver activated zinc sulfide has high scintillation efficiency, and when combined with a ^{6}Li coating, it is able to detect thermal neutrons with a comparable efficiency to ^{3}He.

D. Previous Testing

Pacific Northwest National Lab (PNNL) has previously published results of testing they have done of ^{3}He alternatives that were in their prototyping phase against DHS criteria mentioned earlier [5]. The results of testing that they completed are shown in Table 3 where the failed tests are highlighted in red. The first four detectors listed in this table are proportional counters, and the last three are scintillators.

The proportional counters and the ^{6}Li scintillating plastic meet all of the requirements, but all of the other scintillators do not [5]. Li-6 glass fibers do not meet the requirements for neutron

efficiency due to the low light yield. The Lithium scintillating plastic was the same makeup of the one we tested, however just a prototype. This testing done at PNNL provides a baseline for our measurements as well as metrics to compare our results.

Table 3 – Results reported from PNNL studies of prototype replacement technologies [5]

System Tested	$\varepsilon_{abs,n}$*(cps/ng)*	$\varepsilon_{int\ \gamma,n}$	*GARRn*
DHS Requirement [4]	**2.5**	**$x \leq 10^{-6}$**	**$0.9 \leq x \leq 1.1$**
^{3}He Proportional Counter	3.0	$8x10^{-8}$	1.00
^{10}B Lined Proportional Counter	3.0	$6x10^{-9}$	1.02
$^{10}BF_3$ Filled Proportional Counter	3.7	$6\ x10^{-9}$	N/A
^{10}B Lined Straw Tubes	4.2	$1.5\ x10^{-9}$	1.00
^{6}Li Glass Fibers	1.7	$1\ x10^{-8}$	1.07
^{6}Li/ZnS:Ag Coated Scintillating Fibers	4.0	$1.6\ x10^{-8}$	1.05
^{6}Li/ZnS:Ag Non-scintillating Plastic Fibers	2.4	$5.8\ x10^{-7}$	1.71

E. Systems Being Tested

The scintillator investigated in this work is based on a ^{6}LiF compound dispersed in a matrix of ZnS(Ag) inorganic crystal scintillator with a thickness of about 0.6 mm. Thermal neutrons interact via the ^{6}Li(n, α)^{3}H reaction, and the emergent alpha particles or tritons excite the scintillator [7]. Energy dissipation of the radiated particles within the scintillating medium results in the emission of photons in the ultraviolet of visible wavelength range by electronic de-excitation. This light must then be collected by a PMT by way of a light pipe to amplify the electronic signal into a detectable pulse. Due to the small thickness of ^{6}Li, a degree of gamma discrimination is achieved because a large portion of secondary electrons created by gamma ray interactions will escape without depositing their full energy. This is important to the pulse height discrimination method. The less energy that is deposited by gamma ray interactions, the better the pulse height spectrum can be discriminated against gamma, and neutron interactions due to the differences in energy [7]. Figure 2 shows the ^{6}Li module that was tested [13].

The Aspect Lithium-6 module came directly from Aspect's RPMs, designed to "plug-and-play" with their RPMs rather than be used as a solitary neutron detector. Some reverse-engineering was necessary to communicate through its 9-pin connector without vendor-proprietary hardware. A high voltage power supply was used to power the box and a RS-232 to USB setup was needed in order to connect the monitor to a computer. Software from Aspect was used for data acquisition.

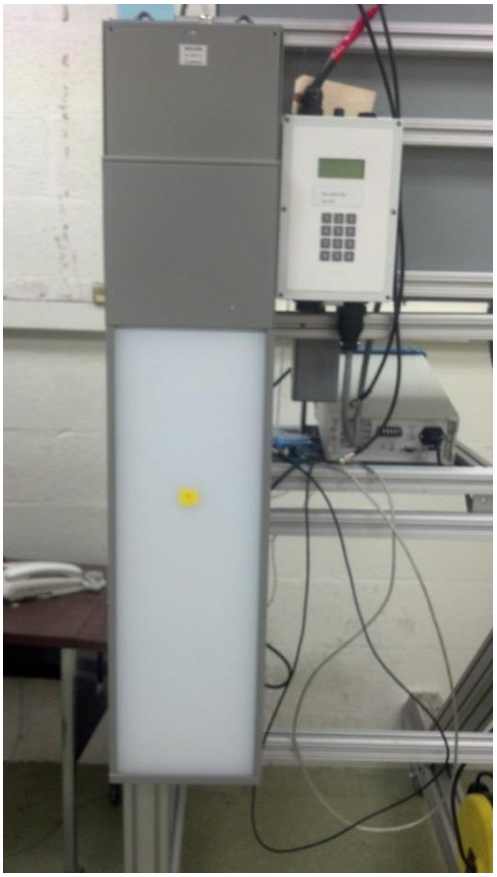


Figure 2 – Li:ZnS(Ag) detector from Aspect

In this work, the testing of Aspect's ^{6}Li:ZnS(Ag) detector [13] will be reported on. This detector has been deployed into the field, and is currently being used for various applications. There has previously been work characterizing this material and different prototype detectors [5,

8, 13], but there has not been significant work done characterizing any deployed systems that use Lithium-6. Most notably there has been no published work done on the response of a detector as a source moves linearly past it, as would be seen by an RPM. Some basic results on the Aspect module have been tested in the past in [13], but for the most part the testing reported in this thesis will be dissimilar. The detectors tested were designed to be used in nuclear security applications, including RPMs. This response (or profile) of the detectors is important to know for characterizing how the RPM will work in real-world applications by predicting the efficiency of the detector as well as finding the periphery of the detectors field of view . Along with this detector, a ^{3}He neutron module taken from a TSA (Rapiscan) RPM was tested alongside it for comparison. The TSA systems configuration is two 2" Helium-3 detectors with a pressure of 2 atm surrounded by a box of polyethylene moderator, where the layer of polyethylene is 1.5 cm thick. It is important to note that this configuration was used to meet a standard, and not to optimize the system. Figure 3 shows the TSA ^{3}He module tested. Over the course of the testing there were some issues that were able to be overcome as well as some that we could not. We originally wanted to test a Boron-10 module, but just as the first testing was to start it became unresponsive and was unable to take any meaningful measurements. It has since been returned to the manufacturer for repair, but was unable to be considered for the following tests. The details about the detector have been included in Appendix A.

There were a few issues that were encountered over the course of setup of the Lithium-6 module. The software provided to us by Aspect to run their modules as a solitary instrument on a computer allowed no way of recording counts anywhere. The software only showed the number of counts collected over the last ten seconds and overwrote it every ten seconds. This required

manual recording all of the counts received from the software into a Microsoft Excel document for analysis.



Figure 3 – TSA Helium-3 module with front cover of moderator box removed

II. EXPERIMENTAL METHODS AND PROCEDURE

Experimental testing for this project was done at Oak Ridge National Laboratory in Oak Ridge, Tennessee. An aluminum cart was repurposed and added onto in order to make a mobile testing center where both the TSA ^{3}He and the Aspect ^{6}Li detectors and electronics could be mounted for testing as shown in Figure 4. The detector centerlines are one meter apart from each other and are located one meter above the floor in order to reduce scatter.



Figure 4 – Testing Cart with mounted Lithium-6 (left) and Helium-3 (right) modules

A. Test 1: Absolute Neutron Detection Efficiency and Radial Response

With the detectors set up one meter apart, we placed two co-located Cf-252 sources (combined strength: 1.42×10^5 n/s ± 0.14%) one meter away from the Aspect detector, and three meters to the left. Starting from the left side (as in Figure 5), we then took 100 s measurements, moving the source 50 cm to the right after every measurement. We took nine measurements total for each detector in order to create a profile response for each, emulating a car driving through the portal.

The absolute neutron detection efficiency was assessed according to the standard described in [4]. Following this standard we placed the same sources together two meters away from each detector and took a 100 s count. All measurements were recorded as average background subtracted net counts per second

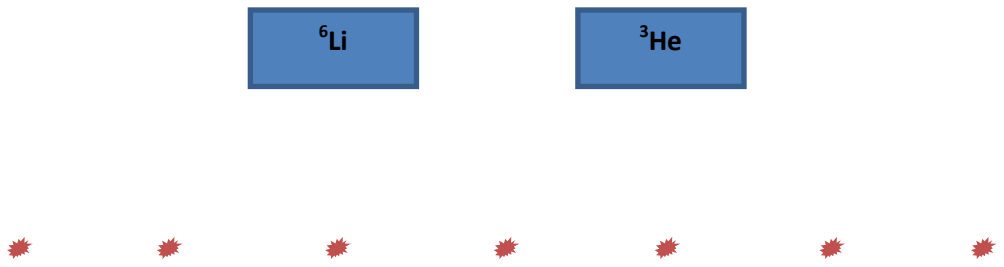


Figure 5 – Illustration of the source progression during the first part of test one

B. Test 2: Gamma Absolute Rejection Ratio for Neutrons

Using a similar setup with the cart, compared with the second part of Test 1, we placed a Cf-252 source (strength reduced to 1.22e5 n/s) one meter from each detector face (in separate experiments for each detector) and a Cs-137 source (~2 mCi) 25 cm from each detector face. This Cesium source produced a gamma field on the detector of 10.03 mR/hr at 25 cm which was

more than enough to exceed the standard of testing of 10 mR/hr. We took a 100 s measurement at this starting location, and then we proceeded to move the gamma source in 5 cm increments closer to each detector face, taking equal duration measurements at each increment.



Figure 6 – Photo of the gamma source on a stand in front of the Lithium-6 module

C. Test 3: Moderation Response

Using a similar static setup as in previous tests, we placed a Cf-252 (strength: 1.22e5 n/s) one meter from each detector (in separate experiments) and took a baseline measurement at each of those points. We then added increasing thicknesses of nested polyethylene spheres to the source to see how the detectors behaved to increasing amounts of source shielding. The

thicknesses of polyethylene used were (in cm): 1.0, 2.5, 4.0, 5.5, 7.0, and 8.5. Figures 7 and 8 show the setup and the spheres used.



Figure 7 – Nested polyethylene spheres for testing



Figure 8 – Photos of the spheres setup for testing: Californium source (left), smallest sphere (center), and largest sphere (right)

D. Test 4: Environmental Testing

Using the Thermal Product Solutions Tenney environmental chamber located at ORNL, we were able to environmentally test the detection modules across a range of temperatures. In order to be conservative and not render the detectors unusable after the testing, we did not test the full range of temperatures described in [4]. We did, however, test in the range from -30 ^{o}C to 60 ^{o}C which encompasses much of the temperature range described in that document. We placed both modules in the test chamber, one meter apart lying on an aluminum table located 75 cm above the floor in order to prevent scatter. A Cf-252 source (strength: 1.04×10^{4} n/s) was mounted on a stand (shown in Figure 9) at a height of one meter above the two detectors, located directly in the center of them. We then took a 4 minute measurement at each 10 ^{o}C temperature step, both with the source and without the source, in order to get a proper Figure of Merit for each detector. Figure of Merit was calculated using equation 4:

$$FOM = \frac{Source\,Counts - Background}{\sqrt{Background}} \tag{4}$$

We chose to calculate the FOM for the temperature testing only because the standard for the profile curve was in net counts, and the GARRn is an absolute measurement. FOM provided a good comparison between the modules for temperature testing since we had a good idea how the Helium-3 module would perform, but wanted to compare it with the Lithium-6 module.

Figure 10 shows the setup of the detectors while they were in the environmental testing chamber. For each programmed change in temperature, the chamber was ramped at 5^{o}C per hour and then allowed to soak at the desired measurement temperature for a period of two hours before the next measurement in order to ensure the modules had reached steady state temperature.

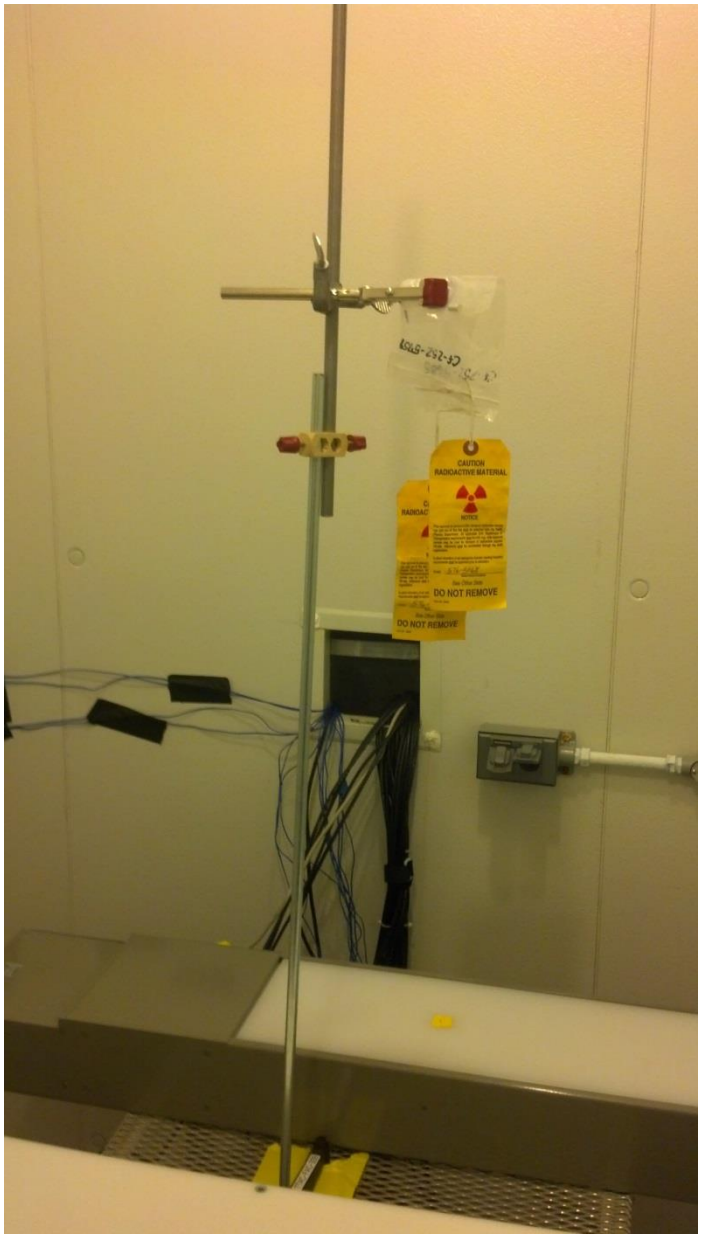


Figure 9 – Photo of the source stand inside the environmental testing chamber

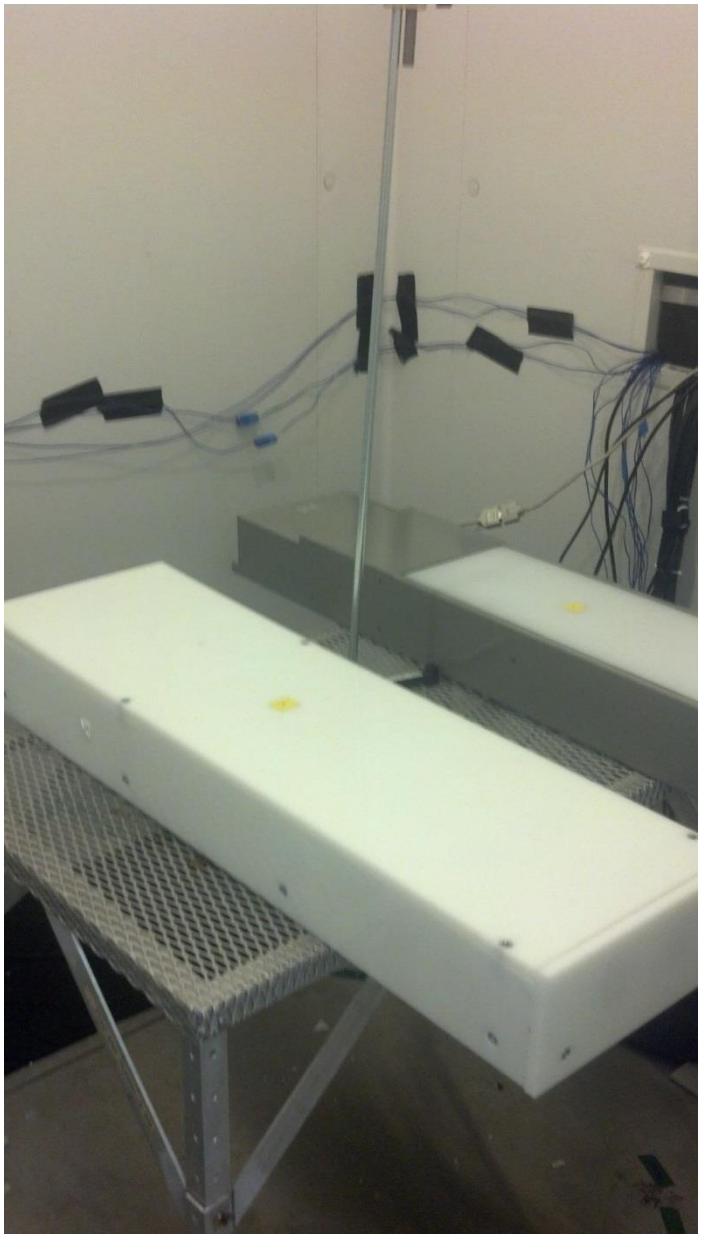


Figure 10 – Helium-3 (left) and Lithium-6 (right) modules setup in the test chamber

III. RESULTS AND DISCUSSION

Data was taken using the native software for both the TSA and Aspect modules. This data was then transferred to a spreadsheet where it was interpreted and sent to Matlab for plotting. All tabular data for the following plots can be found in Appendix B. Error bars were added to the plots where applicable, and were calculated using standard error with a 95% confidence interval as shown in equations 5-7. First the standard deviation needs to be calculated for the data where x is a single measurement for the Lithium-6 or Helium-3 module of five seconds, or one second respectively and x-bar is the average of all the measurements taken represented by n.

$$S = \sqrt{\frac{\sum \left(x - \bar{x}\right)^2}{n-1}} \tag{5}$$

The standard deviation is then converted to the standard error about the mean by dividing by the square root of the number of measurements.

$$S_{\bar{x}} = \frac{S}{\sqrt{n}} \tag{6}$$

In order to get a 95% confidence interval for the measurements, the standard error about the mean needs to be multiplied by 1.96.

$$95\% Confidence = 1.96 S_{\bar{x}} \tag{7}$$

This gets the upper and lower bounds of each measurement point within a confidence interval of 95%.

A. Test 1: Absolute Neutron Detection Efficiency and Radial Response

By first looking at the absolute neutron detection efficiency in Table 4, it is clear that the efficiency of both modules are well within the standards (described in the introduction) of $\varepsilon_{abs,\,n} \geq$

1.2e-5. The intrinsic efficiency was estimated by taking the net counts received by each detector and dividing by the number of neutrons incident on the detection medium. The number of neutrons incident on the detection medium was calculated using Monte Carlo simulation. Figure 11 shows that the Lithium-6 module is about 8% less efficient then the Helium-3 module at the center point of each detector. This plot shows a very similar response for both modules, and shows that the Lithium-6 module is nearly as efficient as the Helium-3 at all points along the curve, which provides evidence that Lithium-6 could be a replacement to Helium-3. The Asymmetric response of the detectors could be due to room geometry, or changes in background during the testing.

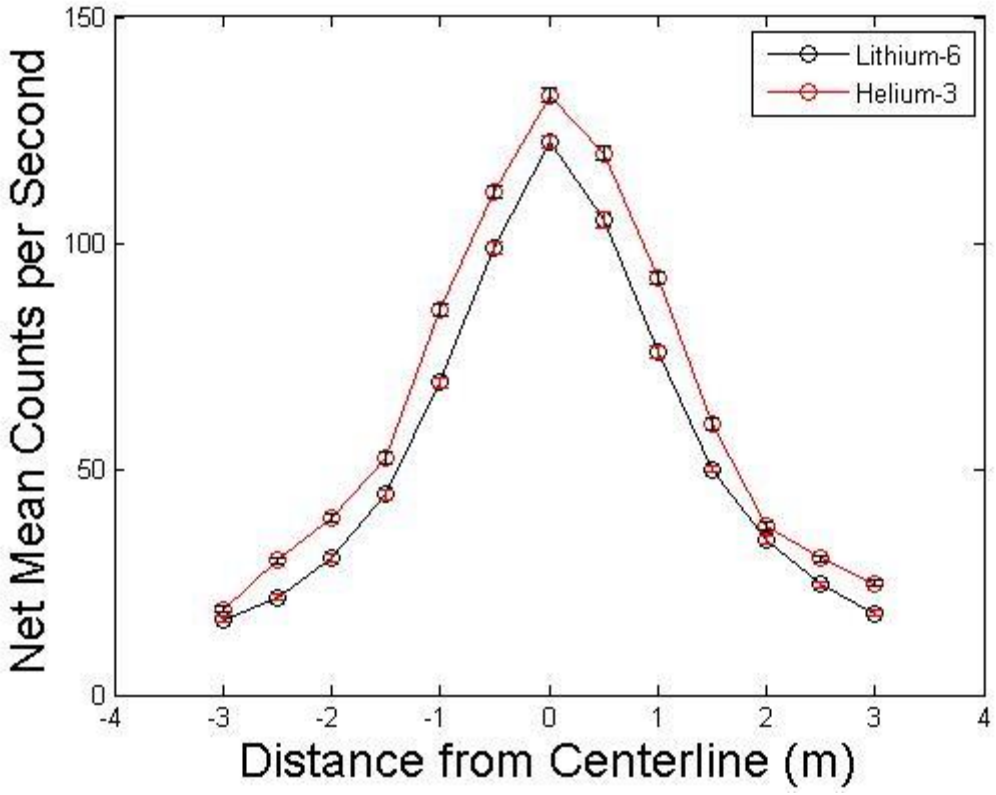


Figure 11 - Plot of the net mean neutron count rate as a source is moved laterally across the face of the detectors where zero is directly in front of the detectors.

Table 4 – Measured absolute neutron detection efficiency for both neutron modules

	Number of Neutrons emitted by source	Net Counts	Intrinsic Efficiency	Uncertainty	**Absolute Neutron Detection Efficiency**	**Uncertainty**
Helium-3	141000	37.3	5.5%	0.21%	**2.6×10^{-4}**	**5.2×10^{-6}**
Lithium-6	141000	33.5	5.4%	0.14%	**2.4×10^{-4}**	**5.8×10^{-6}**

B. Test 2: Gamma Absolute Rejection Ratio for Neutrons

The calculated GARRn value shown in Table 5 is very promising for the Lithium-6 module. This shows that the gamma discrimination of both detectors is within the required limits of: $0.9 \leq x \leq 1.1$. Figures 13 and 14 are shown in order to illustrate these bounds, as well as to visually see the error involved with the two measurements.

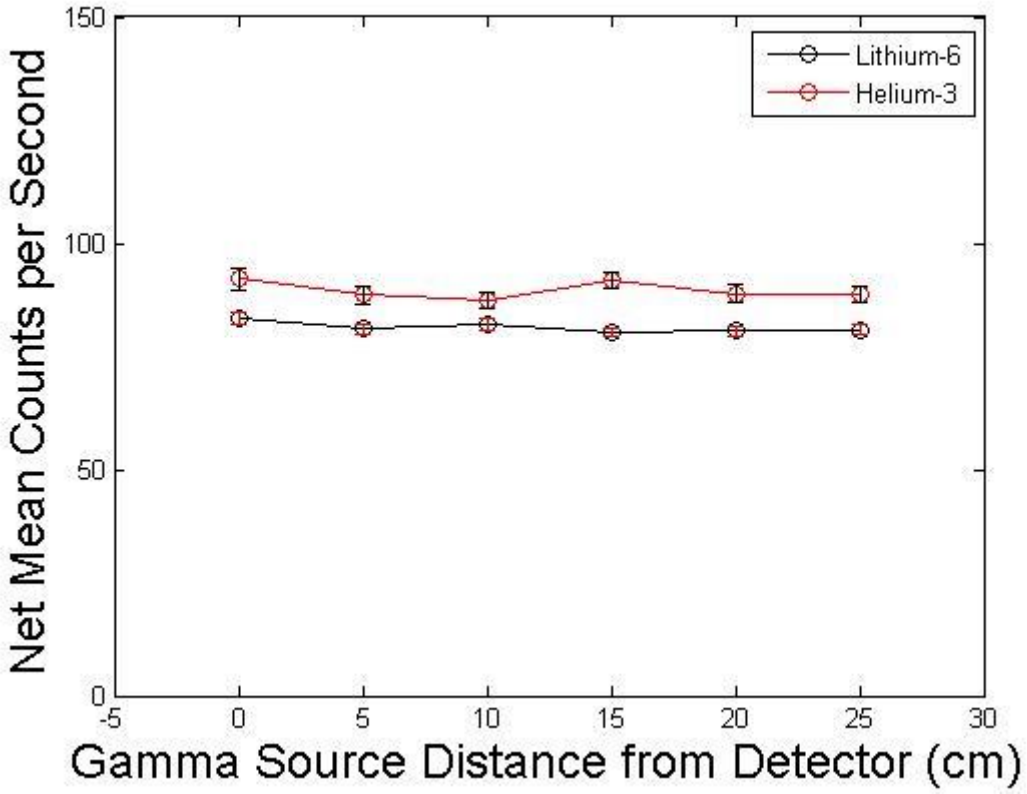


Figure 12 - Mean neutron count rate response of each detector as a gamma source is moved closer to the detector face

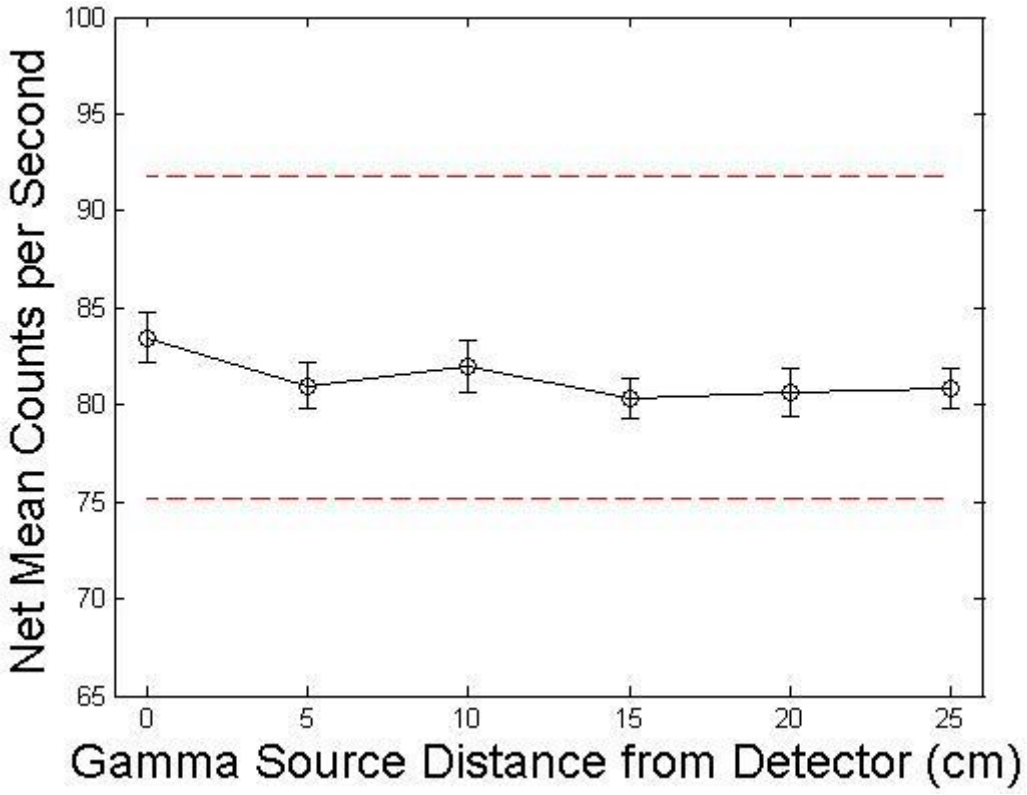


Figure 13 – Zooming in from Figure 12, the mean count rate response of the Lithium-6 module is shown as the gamma source is moved closer to the detector face with error included. The bounds shown in red as outlined in [4] are within 10% of the mean count rate response (83.5 cps) with no gamma source present

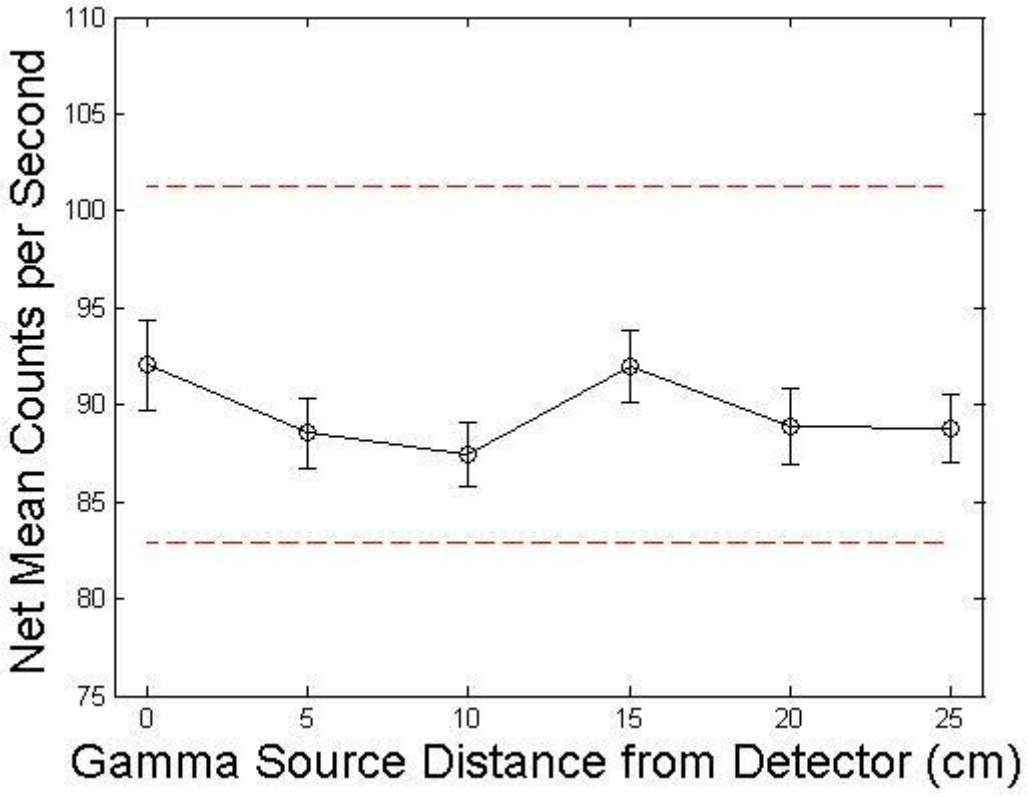


Figure 14 - Zooming in from Figure 12, the mean count rate response of the Helium-3 module is shown as the gamma source is moved closer to the detector face. The bounds shown in red as outlined in [4] are within 10% of the mean count rate response (91.2 cps) with no gamma source present

Table 5 – Gamma Absolute Rejection Ratio for neutrons for both modules

	GARRn	Error(±)
Helium-3	**1.01**	0.03
Lithium-6	**1.00**	0.02

C. Test 3: Moderation Response

Figure 15 shows the change in mean neutron count rate as poly moderator is added to the source. As the data shows, for the Helium-3 module the count rate increases as the moderator thickness increases up until around 6 cm, while the Lithium-6 module begins a decrease in count rate almost immediately. This is due to the way that each company built their detectors. The typical standard [18] for RPMs is to moderate the detectors based upon a bare source, meaning

the detector is working at peak efficiency when there is no moderating material present. This design standard can be seen with the Lithium-6 module. The TSA He-3 module made by Rapiscan, on the other hand, purposefully under-moderates their neutron modules in order to make them more efficient as more moderation is added. In my opinion this was done under the assumption that a nefarious actor would have the foresight to try and shield any material that they were smuggling, increasing the response of the detector. As can be seen, the Helium-3 module has a much better response to increasing amounts of moderation.

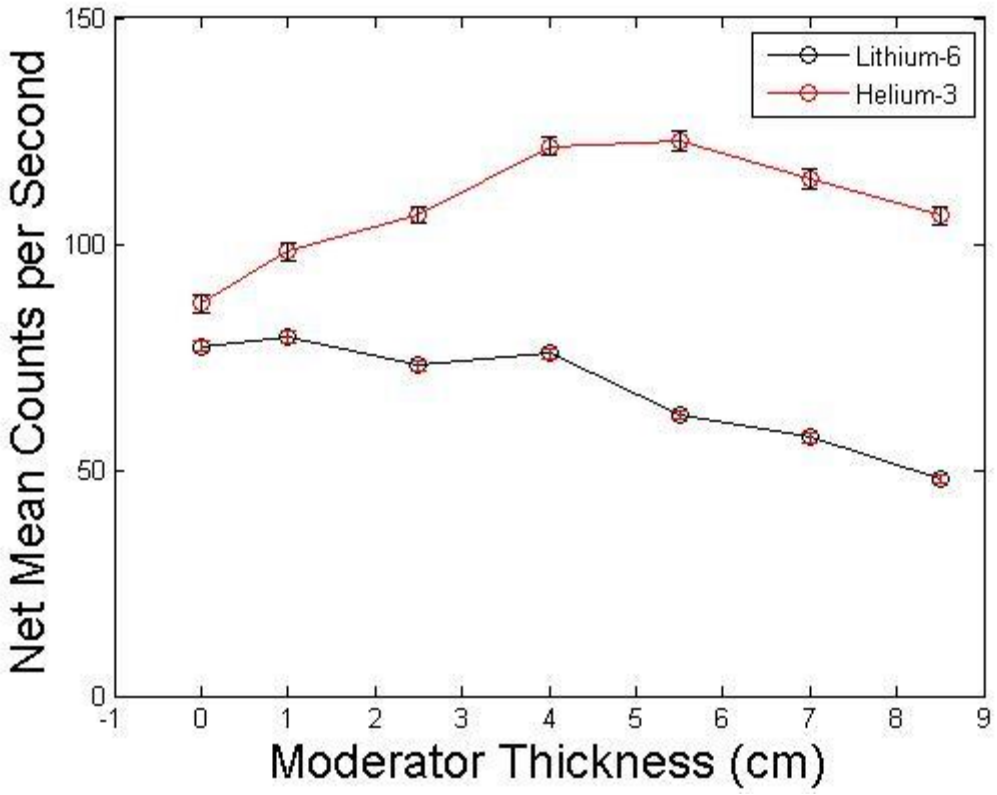


Figure 15 - Neutron response for each module to the addition of increasing thicknesses of polyethylene

D. Test 4: Environmental Testing

Figures 16-18 show the results of environmental temperature testing performed on the detectors at ORNL. From this data, several interesting effects are observed. The desirable

response from a change in temperature is none at all, or a "flat" curve, which is illustrated in Figure 18 by the Helium-3 module data. It can be seen to be flat within the uncertainties shown in that figure. Interestingly, the Lithium-6 module begins to have a slight decrease in the net mean count rate as the temperature increases, decreasing almost 20% over the interval measured. Figure 19 shows a Figure of Merit (FOM) plot for the data in the environmental test [19]. This plot provides a baseline for comparing the two neutron modules as they were in the environmental testing chamber. And it shows that the Lithium-6 module has a higher FOM than the Helium-3 module at all points along the interval. This is due to the slightly higher background that the Helium-3 module measures when compared to the Lithium-6 module. Knowing that the Helium-3 module is under-moderated, the normal efficiency is only about 10% higher than the Lithium-6 module, although its background count rate is about 60% higher. This shows that for both of the modules in their unaltered configurations that the Lithium-6 detector should have a higher FOM.

As can be seen by the data, the Helium-3 module has a much better response to environmental changes in terms of count rate. The decrease in the Lithium-6 count rate with increasing temperature might be attributed to the decrease in the signal-to-noise ratio with increasing temperature within the Photomultiplier Tube (PMT) as stated in the PMT Handbook [14]. This is due to an increase in dark current as the temperature is increased as shown in Figure 20. This count rate decrease due to dark current has been investigated in the past [20, 21], and is well understood. For this experiment the electronics for the Lithium-6 module were placed into the environmental test chamber (As they occupy the same box), but the Helium-3 modules electronics were placed outside of the chamber for convenience of access. This could also lead to some effect from the dark current on the electronics of the detectors. In Figure 16 we can see

that the mean count rate difference for the two detectors is statistically insignificant over the range of -30 ^{o}C to 20 ^{o}C, this is a much different response then the mean neutron count rate shown in Figure 11 where Lithium-6 had a lower mean neutron count rate then Helium-3. This can also be explained by the dark current phenomenon; when the temperature is lower, the less thermal noise there is in the PMT which creates an ideal state for the Lithium-6 module as a whole.

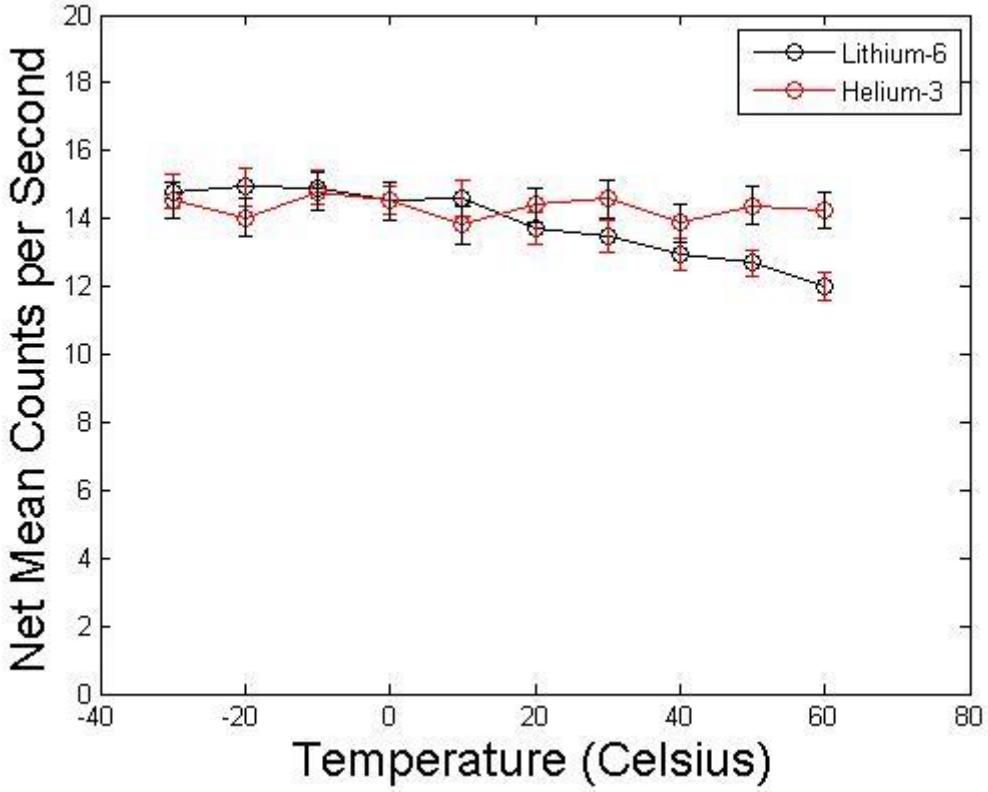


Figure 16 - Mean neutron count rate response for both modules to a change in temperature

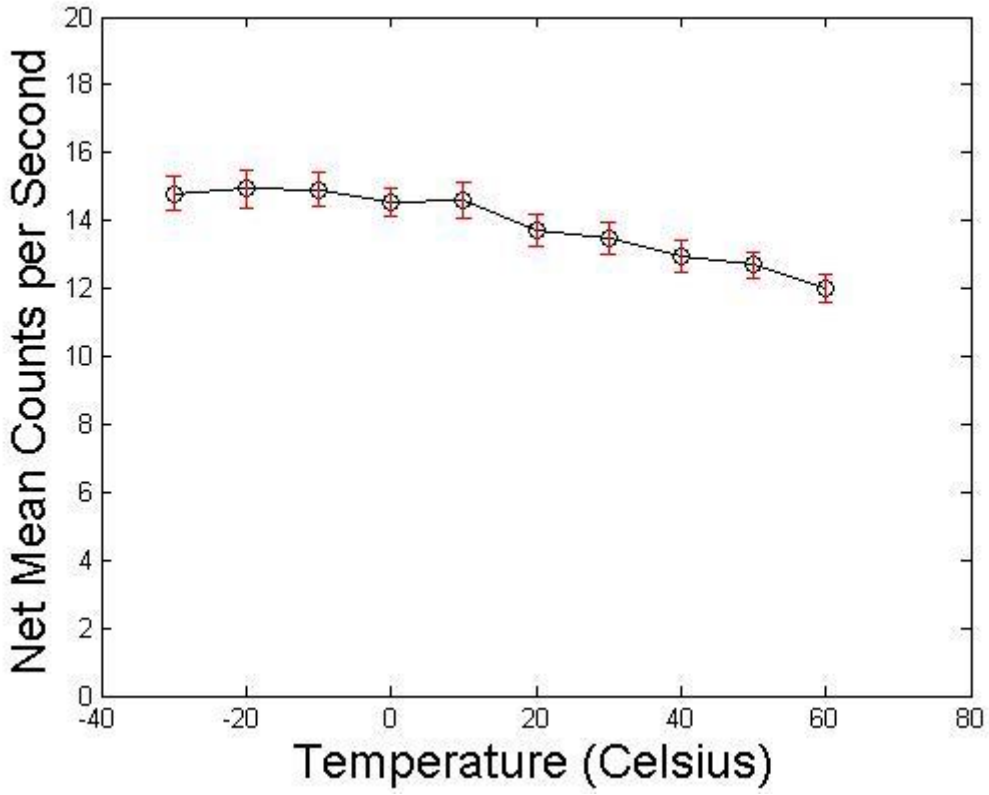


Figure 17 – Mean neutron count rate response for the Lithium-6 module to changing temperature

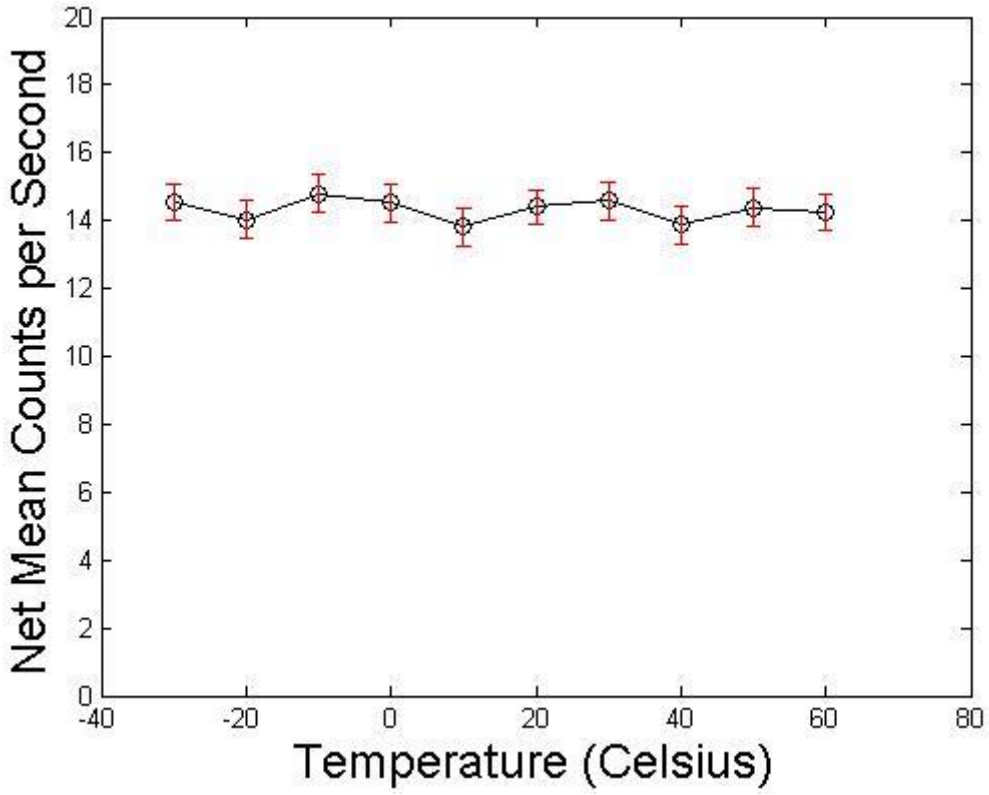


Figure 18 - Mean neutron count rate response for the Helium-3 module to changing temperature

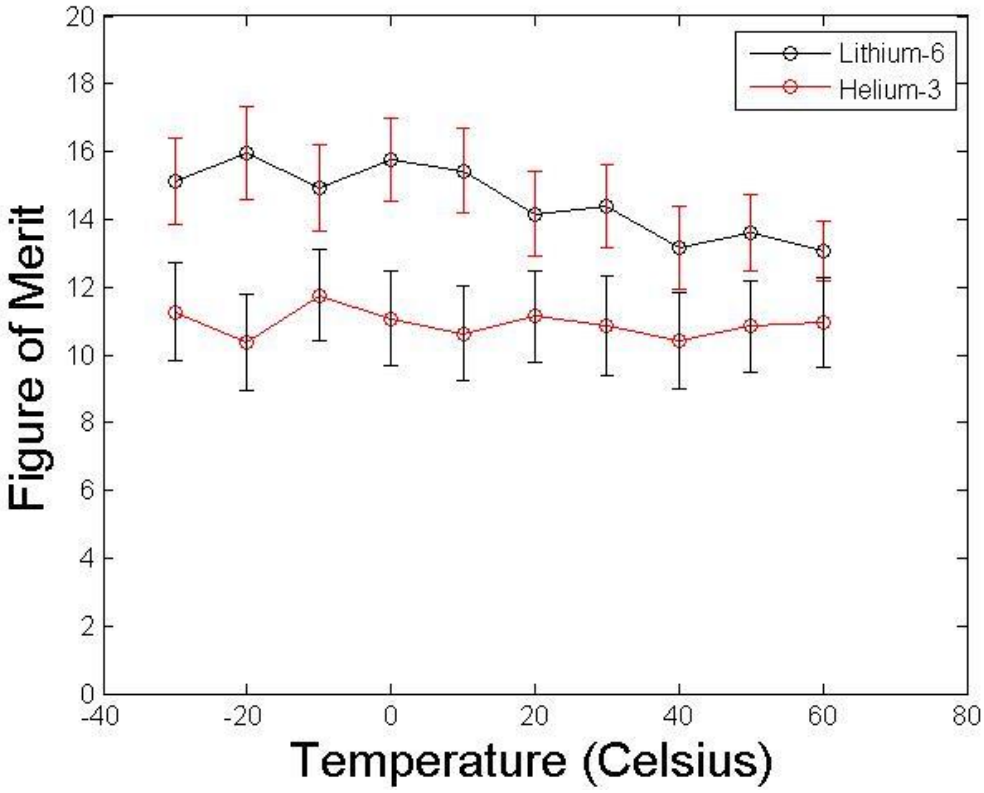


Figure 19 - Figure of Merit for all temperature measurements taken

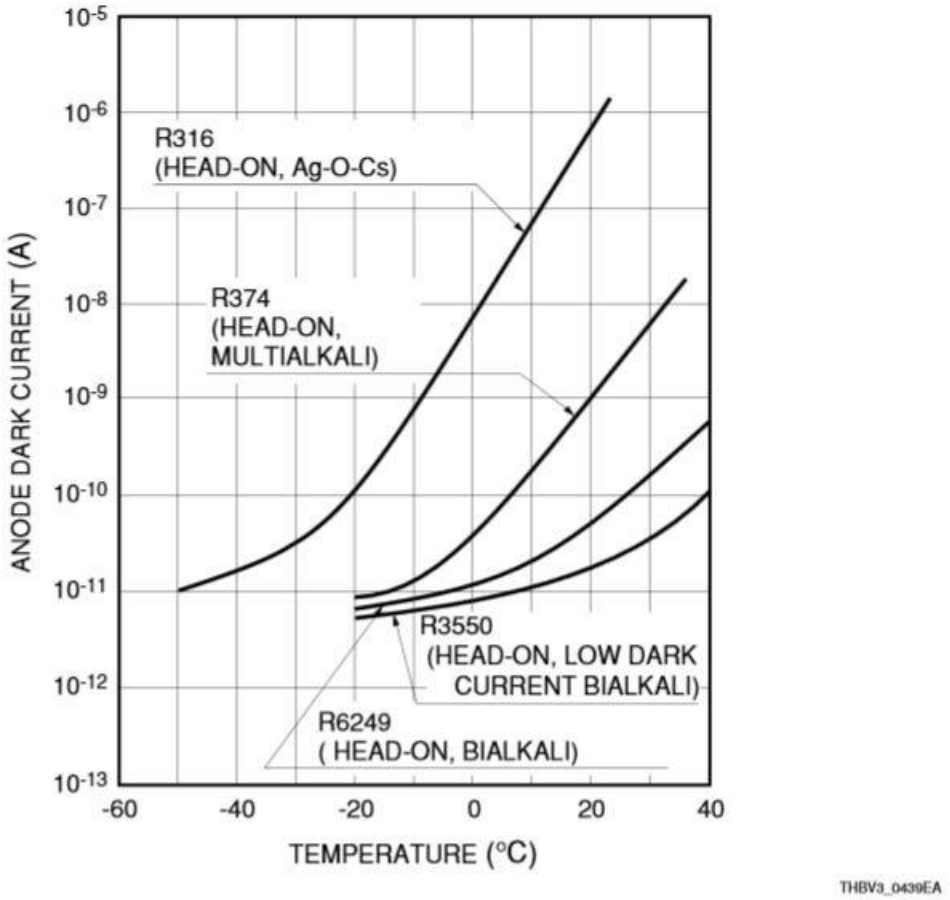


Figure 20 – Plot showing the increase in dark current in a PMT as temperature increases. [14]

IV. MCNP MODELING

Monte Carlo simulation was completed in association with the experimental results received in testing. This allowed us to compare the two results and ensure our Monte Carlo results had been calculated correctly. The Monte Carlo simulations performed for this analysis were done using the Monte Carlo N-Particle code Version 6 (MCNP6). Using this code the detector setups were modeled for Test 1 focusing on the efficiencies and profile curves. Appendix C includes all of the input files used to model these measurements. Table 6 shows the comparison of the absolute neutron detection efficiency from MCNP and our experimental results. Figures 21 and 22 show comparisons of the profiles from Monte Carlo analysis to the experiments. Monte Carlo analysis was also used to model different thicknesses for the front polyethylene plate on the Helium-3 module. This was done in order to find the peak neutron count rate for a Cf-252 source (10000 cps). As can be seen in Figure 23, the peak count rate is expected to occur somewhere between a front plate thickness of 5.2 cm and 5.5 cm. This is consistent with the experimental moderation testing we did where the highest neutron response occurred with a 5.5cm thick polyethylene shell around the source shown in Figure 15.

Table 6 – Comparison of the absolute neutron detection efficiency as taken from experimental results and from Monte Carlo analysis

	Absolute Neutron Detection Efficiency	MCNP Absolute Neutron Detection Efficiency	MCNP Tally Error	Percent Difference
Helium-3	2.6×10^{-4}	2.7×10^{-4}	0.02	3.7%
Lithium-6	2.4×10^{-4}	2.5×10^{-4}	0.02	4.8%

From Table 6 it can be seen that the MCNP results match our experimental results for Helium-3 and Lithium-6 with a percent difference of 3.7% and 4.8% respectively. Not knowing the exact makeup of the Aspect detector created a lot of difficulties, but some references do exist

about other Lithium-6 modules in literature [3, 7]. The models that were created were based upon a Lithium-6 thickness of 0.6 mm found in [7] and a Polyethylene moderator thickness of 3 cm found in [5, 7]. Judging from the results obtained in Table 6, these assumptions proved to be fairly accurate. Figures 21 and 22 show the modeled profile curves against our experimental results. Again these plots support that the output from our experimental measurements is valid. The higher count rates toward the outside for the experimental measurements are probably due to neutron scatter in the room which was not taken into account in the models.

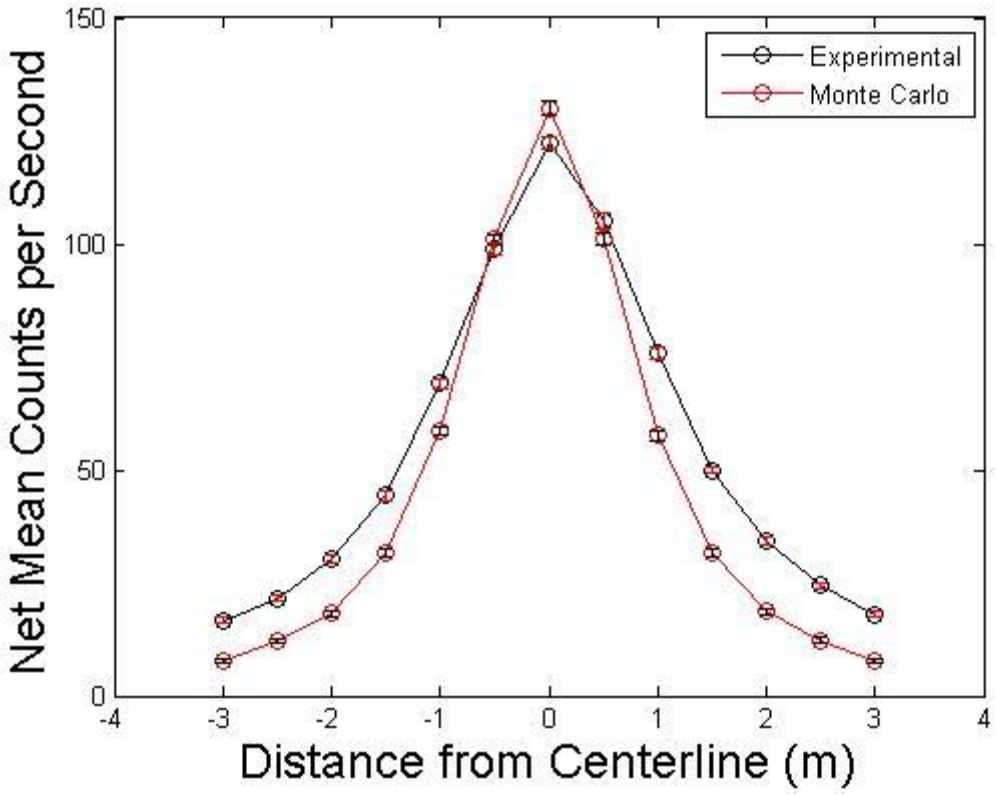


Figure 21 - Comparison between experimental and simulated mean neutron count rate profiles for the Lithium-6 module

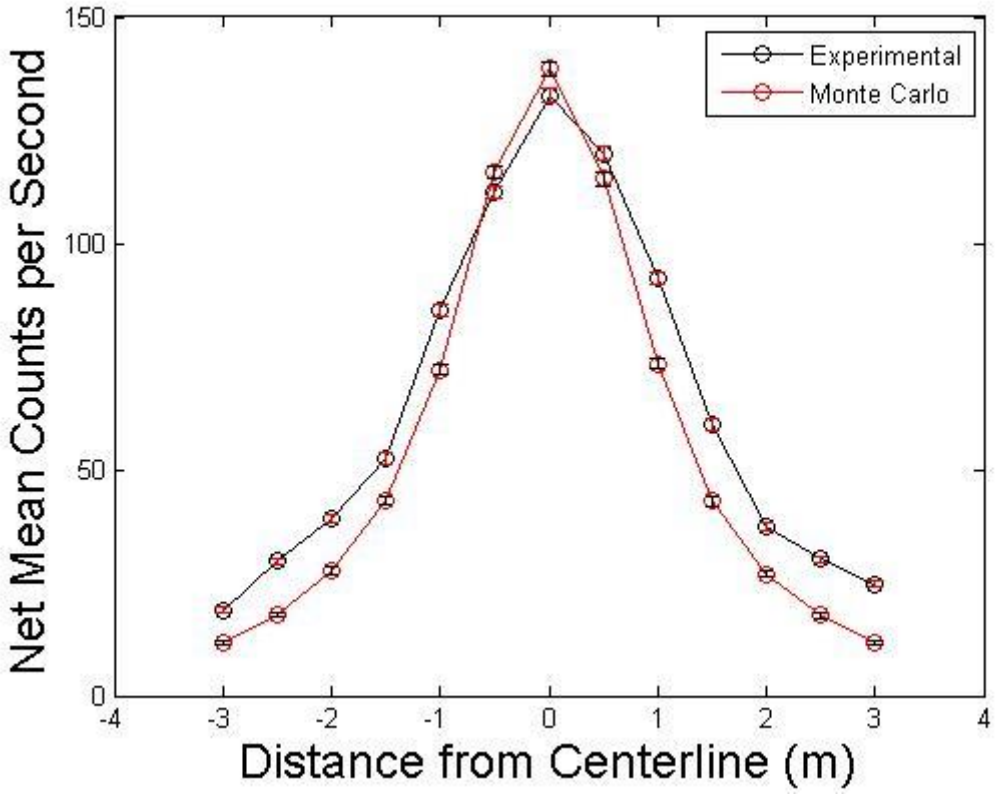


Figure 22 - Comparison between experimental and simulated mean neutron count rate profiles for the Helium-3 module

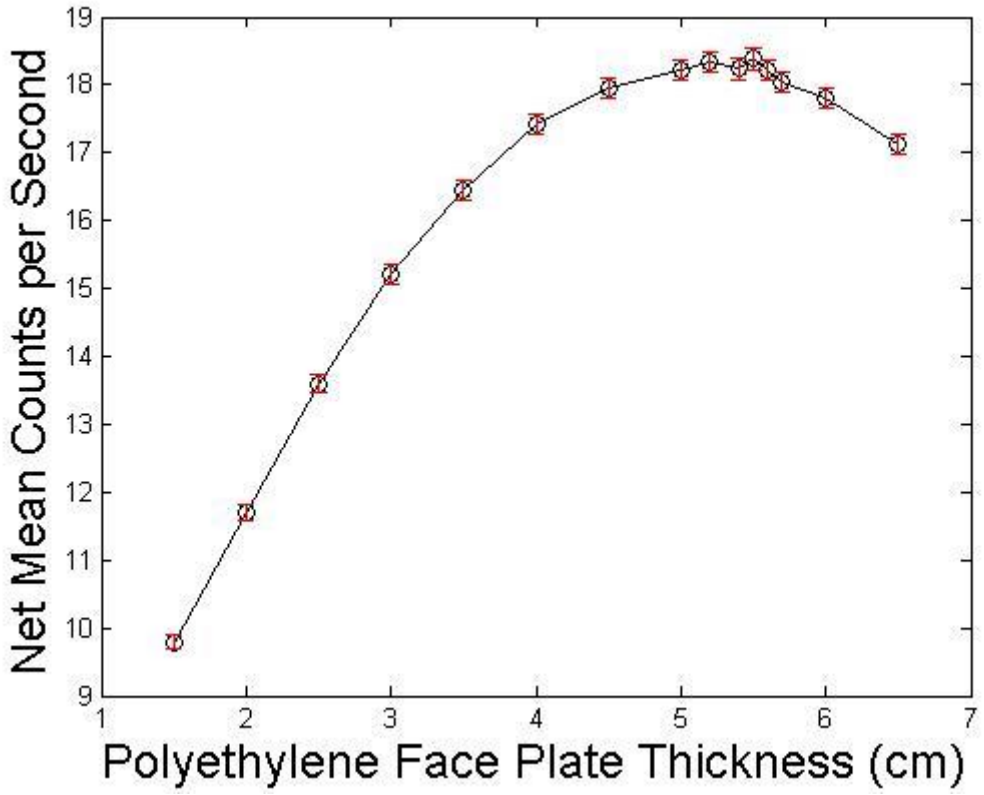


Figure 23 – MCNP simulation of the mean neutron count rate for an increasing thickness of polyethylene moderator face plate on the Helium-3 Module.

V. CONCLUSIONS AND FUTURE WORK

A. *Conclusions*

This work focused on the testing and benchmarking of ^{6}Li:ZnS(Ag) as a replacement for helium-3. During the experimentation process we were able to directly compare a Lithium-6 detector from Aspect Technologies against a currently employed Helium-3 detector from TSA Systems. The findings reported in this thesis suggest that Lithium-6 is a viable alternative to Helium-3 based upon the metrics specified of: 1) high absolute detection efficiency, 2) maintaining neutron detection efficiency when simultaneously exposed to high gamma ray exposure rate, and 3) the ability to maintain neutron detection rate in all operational temperature ranges. Of these metrics, Lithium-6 met all of the requirements of alternatives specified in the DNDO document that we tested [4]. Table 7 shows the calculated values for all of the metrics that we were testing along with the requirements. From this table it can clearly be seen that the Lithium-6 Aspect detector is very viable for the replacement of Helium-3 in Radiation Portal Monitors throughout the world.

Table 7 – Table outlining the requirements and experimental data for neutron efficiency and GARRn

	Absolute Neutron Detection Efficiency	*Gamma Absolute Rejection Ratio for Neutrons*
Requirement	$\boldsymbol{\varepsilon_{abs,n} \geq 1.2 \times 10^{-5}}$	$\boldsymbol{0.9 \leq x \leq 1.1}$
Lithium-6	$2.4 \times 10^{-4} \pm 0.052 \times 10^{-4}$	1.01 ± 0.03
Helium-3	$2.6 \times 10^{-4} \pm 0.058 \times 10^{-4}$	1.00 ± 0.02

B. *Suggested Future Work*

Future testing of different alternatives could be done using the outlined methods in this paper to compare them against the Lithium-6 and Helium-3 modules tested in this thesis. I would have really liked to test the Boron-10 module alongside of the others for comparison and

benchmarking. MCNP modeling of different detector setups could also be done to find the most efficient detector configurations for the tested modules as well as other alternatives that are currently available. Along with testing other detectors, humidity, electromagnetic response, vibration, dust, and other environmental testing should be looked at for all of the currently available detectors.

BIBLIOGRAPHY

[1] Richard T. Kouzes, "Neutron Detection Alternatives to He-3 for National Security Applications," Nuclear Instruments and Methods in Physics Research A, vol. 623, pp. 1035-1045, August 25, 2010.

[2] United States Government Accountability Office, "Neutron Detectors - Alternatives to using Helium-3," Center for Science, Technology, and Engineering, September 2011.

[3] R.T. Kouzes, M. Wright, R.K. Crawford, J.L. Robertson (ORNL), in: The 3He supply problem and possible alternative technology, Technical Rpt. PNNL- 18550, Pacific Northwest National Laboratory, Richland, WA, 2009

[4] United States Department of Homeland Security, "Functional Requirements Document For Radiation Portal Monitor System ^{3}He Neutron Detection Module Replacement" Domestic Nuclear Detection Office, April 28, 2010, Document Number: 600-NDRP-113410v2.07

[5] R.T.Kouzes, in: The 3He supply problem, Technical Rpt. PNNL-18388, Pacific Northwest National Laboratory, Richland, WA, 2009.

[6] A.T. Lintereur, R.T. Kouzes, J.H. Ely, L.E. Erikson, E.R. Siciliano, and M.L. Woodring in: Boron-Lined Neutron Detector Measurements Technical Rpt. PNNL- 18938, Pacific Northwest National Laboratory, Richland, WA, 2009

[7] Knoll, Glenn F. *Radiation Detection and Measurement*. Hoboken, NJ: John Wiley, 2010.

[8] Matthew Dallimore, "The Development of a He-3 Free Neutron Detection Technology and its Potential Use in Nuclear Security and physical protection applications", Symetrica Inc. Report. Maynard, MA, 2010.

[9] Jeffery L. Lacy, "Performance of a Straw based Portable Neutron Coincedence Counter," IEEE Nuclear Science Symposium Conference Record, pp. 529-532, 2011.

[10] B.M. Young, "Estimation of Performance of an Active Well Coincidence Counter Equipped with Boron-Coated Straw Neutron Detectors," WM2013 Conference Proceedings, February 28, 2013.

[11] Jeffery L. Lacy, "Design and Performance of High-Efficiency Counters Based on Boron-Lined Straw Detectors," INMM 2012 Conference Proceedings, September 3, 2013.

[12] J.L. Lacy, A. Athanasiades, C.S. Martin, L. Sun, and G.J. Vazquez-Flores, "Straw-based-portal monitor ^{3}He replacement detector with expanded capabilities", IEEE 2011 Nuclear Science Symposium Conference Record, (2011), pp. 4865-4868.

[13] Christopher Lovejoy, "Aspect LiZnS Neutron Detector Evaluation," Los Alamos Controlled Publication, vol. LA-CP-12-01345, October 22, 2012.

[14] Hamamatsu "Photomultiplier Tubes Basics and Applications" 3rd Edition, 2006

[15] Martin, R.C., "Production, Distribution, and Applications of Californium-252 Neutron Sources", September 30, 1999. Available at http://web.ornl.gov/~webworks/cpr/pres/102606.pdf?origin=publication_detail .

[16] Bondarenko, L. N.; Kurguzov, V. V.; Prokof'ev, Y. A.; Rogov, E. V.; Spivak, P. E. *Pis'ma Zh. Eksp. Teor. Fiz.* **1978**, *28*, 328.

[17] Spowart, A. R. *Nucl. Instrum. Meth.* **1976**, *135*, 441.

[18] American National Standard for Evaluation and Performance of Radiation Detection Portal Monitors for Use in Homeland Security," *ANSI N42.35-2006* section 7, Jan. 22 2007

[19] Fehlau, P.E., "An Application Guide to Pedestrian Portal Monitors" Los Alamos Publication, vol. LA-10633-MS, February 1986

[20] Addington, D.J., Baird, Chiaro, Enders, Livesay, York, "An Evaluation of the Sensitivity of Rail RPM Components to Temperature Variations" Oak Ridge National Laboratory Controlled Document, ORNL/TM-2011/526, January 2012

[21] Addington, D.J., Baird, Chiaro, "Temperature Test Report for a Pedestrian RPM used in Nuclear Security Applications" Oak Ridge National Laboratory Controlled Document, ORNL/TM-2011/128, December 2011.

[22] Voss, J.T., "Radiation Monitoring Notebook" Los Alamos Publication, LA-UR-00-2584, June 2000

APPENDICES

Appendix A: Other Detectors Analyzed

Boron Coated Straw

The boron-coated straw (BCS) detector is based on close-packed arrays of thin-walled, boron-coated aluminum or copper tubes. The tube is coated on the inside with a thin layer of ^{10}B-enriched boron carbide ($^{10}B_4C$). Thermal neutrons captured in ^{10}B are converted to secondary particles, through the $^{10}B(n,\alpha)^7Li$ reaction [7, 10, 11, 12]. The ^{7}Li and α particles are emitted isotropically in opposite directions with kinetic energy of 1.47 MeV and 0.84 MeV, respectively. For a 1 μm thick boron carbide layer, one of the two charged particles will escape the wall about 78% of the time, and it will ionize the gas contained within the straw. A detector consisting of 143 close-packed straws, as shown in Figure 24, offers a stopping power for neutrons equivalent to that of approximately 2.68 atm of ^{3}He gas when sampling a thermal neutron field configuration. Figure 25 shows the ^{10}B model that was tested. The geometry of the B-10 detector is not optimized for our purposes due to it not being in an RPM module form, but it is readily available for test.

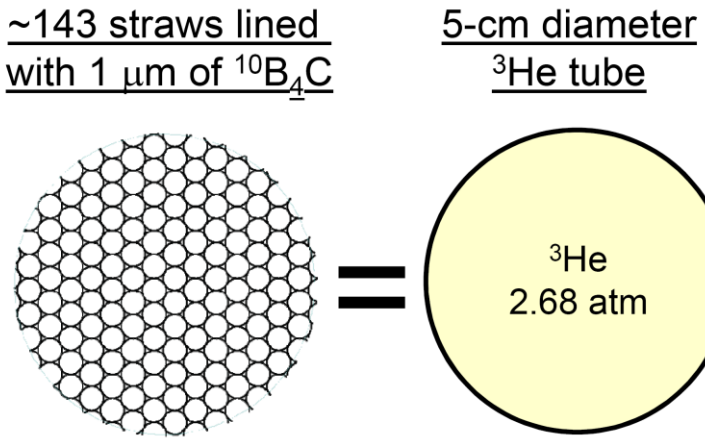


Figure 24 – Stopping power equivalence between straw detectors (4mm diameter) lined with 1 μm of $^{10}B_4C$, and ^{3}He gas. [10]

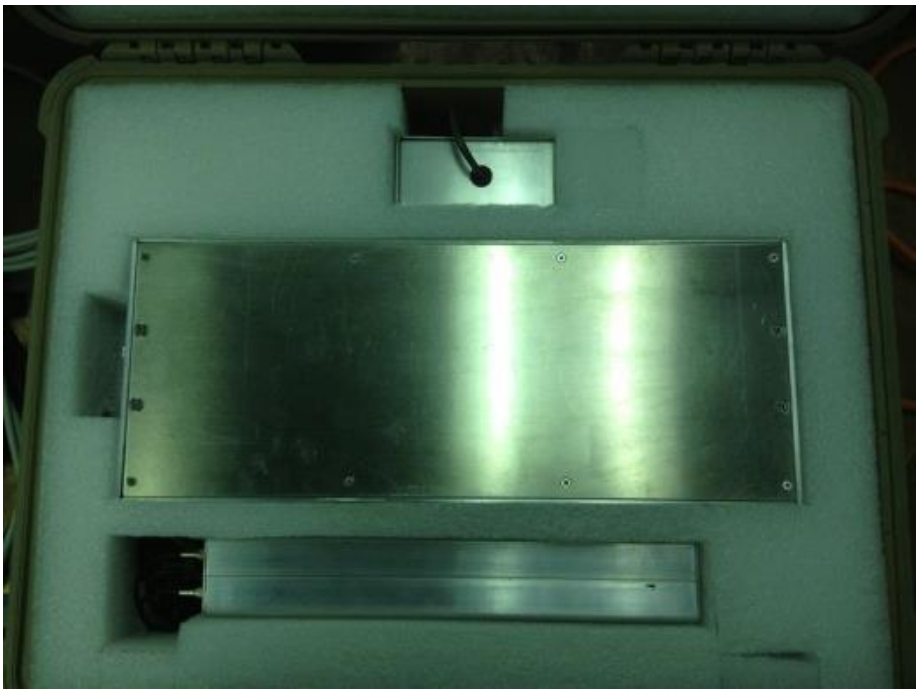


Figure 25 – Photo of the electronics and BCS detector all contained within a Pelican case

Unlike the scintillator, our detector from PTI is designed to work as a correlated neutron counter, alarming when it detects an increase in the time-correlated number of neutrons. It is deployed in a pelican case for portability when taken into the field. Figure 26 shows the original testing setup with the PTI module to the far left.



Figure 26 – Full testing setup with the Boron-10 (left), Lithium-6 (center), and Helium-3 (right) modules

Appendix B: Tabular Data from Plots

Test 1: Absolute Neutron Detection eEficiency and Radial Response

Table 8 – Net mean neutron count rate for neutron profile

Distance from Centerline (meters)	Helium-3		Lithium-6	
	Net Mean Counts per Second	Error (±)	Net Mean Counts per Second	Error (±)
-3.0	18.94	0.65	16.77	0.61
-2.5	29.66	0.75	21.53	0.69
-2.0	38.99	0.86	30.39	0.98
-1.5	52.45	1.17	44.41	1.15
-1.0	85.36	1.30	69.10	1.13
-0.5	111.28	1.39	98.76	1.33
0.0	132.68	1.51	122.27	1.36
0.5	119.81	1.44	105.10	1.60
1.0	92.45	1.33	75.86	1.20
1.5	59.92	1.19	49.98	0.83
2.0	37.35	1.03	34.19	0.77
2.5	30.13	0.75	24.37	0.71
3.0	24.61	0.71	18.09	0.64

Test 2: Gamma Absolute Rejection Ratio for Neutrons

Table 9 – Net mean neutron count rate for response to a gamma source

Gamma Source Distance (cm)	Helium-3		Lithium-6	
	Net Mean Counts per Second	Error (±)	Net Mean Counts per Second	Error (±)
Baseline	91.16	2.01	83.49	1.18
25	88.77	1.78	80.85	1.02
20	88.86	1.96	80.62	1.23
15	91.96	1.84	80.31	1.01
10	87.48	1.65	81.95	1.36
5	88.53	1.85	81.00	1.19
0	92.06	2.31	83.47	1.26

Test 3: Moderation Response

Table 10 – Net mean neutron count rate for moderation response

Polyethylene Thickness (cm)	Helium-3		Lithium-6	
	Net Mean Counts per Second	Error (±)	Net Mean Counts per Second	Error (±)
0.0	86.73	1.87	77.38	1.08
1.0	98.30	1.88	79.44	1.27
2.5	106.44	1.62	73.09	1.04
4.0	121.68	2.17	75.67	0.93
5.5	122.85	2.19	62.21	0.87
7.0	114.34	2.04	57.09	1.11
8.5	106.22	2.08	48.00	0.88

Test 4: Environmental Testing

Table 11 – Net mean neutron count rate for environmental testing

Temperature (^{o}C)	Helium-3		Lithium-6	
	Net Mean counts per Second	Error (±)	Net Mean counts per Second	Error (±)
-30	14.55	0.52	14.80	0.49
-20	14.03	0.56	14.93	0.58
-10	14.79	0.56	14.93	0.51
0	14.54	0.56	14.54	0.43
10	13.81	0.55	14.60	0.54
20	14.40	0.51	13.69	0.47
30	14.58	0.57	13.48	0.50
40	13.87	0.57	12.94	0.46
50	14.39	0.56	12.69	0.38
60	14.25	0.52	12.00	0.42

Appendix C: MCNP Input Files

Helium-3 Profile Base Input

```
c    ********************************************************************************
c    cells
c    ********************************************************************************
c
  1   1  -0.97    -1                                        imp:n=1  $ LHS
  2   1  -0.97    -2                                        imp:n=1  $ RHS
  3   1  -0.97    -3 #10 #11                                imp:n=1  $ Top
  4   1  -0.97    -4 #10 #11                                imp:n=1  $ Bottom
  5   1  -0.97    -5                                        imp:n=1  $ Back
  6   1  -0.97    -6                                        imp:n=1  $ Front
 10   2  1.002e-4 -10                                       imp:n=1  $ LHS Tube
 11   2  1.002e-4 -11                                       imp:n=1  $ RHS Tube
100   0          -100 #1 #2 #3 #4 #5 #6 #10 #11            imp:n=1  $ World
101   0          100                                       imp:n=0  $ Universe

c    ********************************************************************************
c    surfaces
c    ********************************************************************************
c
c    Polyethylene detector encasement
1   rpp   -14.0 -12.5 1.5 96.5 -13 -1.5                  $ LHS of Box
2   rpp    12.5  14.0 1.5 96.5 -13 -1.5                  $ RHS of Box
3   rpp   -14.0  14.0 96.5 98.0 -13 -1.5                 $ Top of Box
4   rpp   -14.0  14.0 0.0 1.5 -13 0.0                    $ Bottom of Box
5   rpp   -12.5  12.5 1.5 96.5 -13 -10                   $ Back of Box
6   rpp   -14.0  14.0 1.5 98.0 -1.5 0                    $ Front of Box
c
c    Helium-3 Tubes
10  rcc   -4.75 1.5 -5.75  0 95 0  2.54                  $ LHS Detector
11  rcc    4.75 1.5 -5.75  0 95 0  2.54                  $ RHS Detector
100 rpp   -400 400 -10 110 -20 300                       $ Edge of World

c    ********************************************************************************
c       Source Cards
c    ********************************************************************************
c
c ********************************************************************************
c
c     ----------------------------------------------------------------
c       Source
c     ----------------------------------------------------------------
  SDEF ERG=D1 POS=300 49 100
c
  SP1 -2 1.42
c
c
c ********************************************************************************
c
c    ********************************************************************************
c       Material Cards
c    ********************************************************************************
c
c   material-1,  poly
m1   06000.66c     0.33333
       01001.66c     0.66667
mt1   poly.60t
c
c   material-2,  helium-3 gas
m2   02003.66c     1.0
c ********************************************************************************
c
```

```
c    ***************************************************************************
c       Tally Cards
c    ***************************************************************************
c
nps 10000000
mode  n
F4:n (10 11)
sd4 1.0
fm4 -1.0 2 103
c
c END FILE
```

Lithium-6 Profile Base Input

```
c    ***************************************************************************
c    cells
c    ***************************************************************************
c
  1   1  -4.090    -1                          imp:n=1  $ ZincSulfide
  2   2  -0.534    -2                          imp:n=1  $ Lithium
  3   3  -0.93     -3                          imp:n=1  $ Polyethylene
100   0          -100 #1 #2 #3                imp:n=1  $ World
101   0          100                           imp:n=0  $ Universe

c    ***************************************************************************
c    surfaces
c    ***************************************************************************
c
c    Polyethylene detector encasement
1   rpp   -11.5 11.5 0.0 92.0 -12.0 -3.06          $ Zinc-Sulfide  Portion
2   rpp   -11.5 11.5 0.0 92.0 -3.06 -3.00          $ Lithium Portion
3   rpp   -11.5 11.5 0.0 92.0 -3.00 0.00           $ Polyethylene
100 rpp   -400 400 -10 110 -20 300                 $ Edge of World

c    ***************************************************************************
c       Source Cards
c    ***************************************************************************
c
c ***************************************************************************
c
c     ------------------------------------------------------------
c       Source
c     ------------------------------------------------------------
  SDEF ERG=D1 POS=300 46 100
c
  SP1 -2 1.42
c
c
c ***************************************************************************
c
c    ***************************************************************************
c       Material Cards
c    ***************************************************************************
c
c   material-1,  Zinc-Sulfide
m1   16000        0.5
       30000        0.5
c
c   material-2,  Lithium-6
m2   03006        1.0
c
c   material-3,  poly
m3   06000.66c     0.33333
       01001.66c     0.66667
mt3   poly.60t
c ***************************************************************************
```

```
c
c    ***************************************************************************
c       Tally Cards
c    ***************************************************************************
c
nps 10000000
mode  n
f4:n 2
sd4 1.0
fm4 -1.0 2 105
c
c END FILE
```

Helium-3 Efficiency Input

```
c    ***************************************************************************
c    cells
c    ***************************************************************************
c
  1   1  -0.97    -1                                    imp:n=1  $ LHS
  2   1  -0.97    -2                                    imp:n=1  $ RHS
  3   1  -0.97    -3 #10 #11                            imp:n=1  $ Top
  4   1  -0.97    -4 #10 #11                            imp:n=1  $ Bottom
  5   1  -0.97    -5                                    imp:n=1  $ Back
  6   1  -0.97    -6                                    imp:n=1  $ Front
 10   2  1.002e-4 -10                                   imp:n=1  $ LHS Tube
 11   2  1.002e-4 -11                                   imp:n=1  $ RHS Tube
100   0          -100 #1 #2 #3 #4 #5 #6 #10 #11        imp:n=1  $ World
101   0          100                                   imp:n=0  $ Universe

c    ***************************************************************************
c    surfaces
c    ***************************************************************************
c
c    Polyethylene detector encasement
1   rpp   -14.0 -12.5 1.5 96.5 -13 -1.5                $ LHS of Box
2   rpp    12.5  14.0 1.5 96.5 -13 -1.5                $ RHS of Box
3   rpp   -14.0  14.0 96.5 98.0 -13 -1.5               $ Top of Box
4   rpp   -14.0  14.0 0.0 1.5 -13 0.0                  $ Bottom of Box
5   rpp   -12.5  12.5 1.5 96.5 -13 -10                 $ Back of Box
6   rpp   -14.0  14.0 1.5 98.0 -1.5 0                  $ Front of Box
c
c    Helium-3 Tubes
10  rcc   -4.75 1.5 -5.75  0 95 0  2.54                $ LHS Detector
11  rcc    4.75 1.5 -5.75  0 95 0  2.54                $ RHS Detector
100 rpp   -20 20 -10 110 -20 300                       $ Edge of World

c    ***************************************************************************
c       Source Cards
c    ***************************************************************************
c
c ***************************************************************************
c
c     ------------------------------------------------------------
c       Source
c     ------------------------------------------------------------
  SDEF ERG=D1 POS=0 49 200
c
  SP1 -2 1.42
c
c
```

```
c ***************************************************************************
c
c    ***************************************************************************
c        Material Cards
c    ***************************************************************************
c
c   material-1,  poly
m1   06000.66c    0.33333
       01001.66c    0.66667
mt1   poly.60t
c
c   material-2,  helium-3 gas
m2   02003.66c    1.0
c ***************************************************************************
c
c    ***************************************************************************
c        Tally Cards
c    ***************************************************************************
c
nps 10000000
mode  n
F4:n (10 11)
sd4 1.0
fm4 -1.0 2 103
c
c END FILE
```

Lithium-6 Efficiency Input

```
c    ***************************************************************************
c    cells
c    ***************************************************************************
c
  1   1  -4.090    -1                          imp:n=1  $ ZincSulfide
  2   2  -0.534    -2                          imp:n=1  $ Lithium
  3   3  -0.93     -3                          imp:n=1  $ Polyethylene
100   0          -100 #1 #2 #3                 imp:n=1  $ World
101   0          100                           imp:n=0  $ Universe

c    ***************************************************************************
c    surfaces
c    ***************************************************************************
c
c    Polyethylene detector encasement
1   rpp   -11.5 11.5 0.0 92.0 -12.0 -3.06          $ Zinc-Sulfide  Portion
2   rpp   -11.5 11.5 0.0 92.0 -3.06 -3.00          $ Lithium Portion
3   rpp   -11.5 11.5 0.0 92.0 -3.00 0.00           $ Polyethylene
100 rpp    -20 20 -10 110 -20 300                  $ Edge of World

c    ***************************************************************************
c        Source Cards
c    ***************************************************************************
c
c ***************************************************************************
c
c     ------------------------------------------------------------
c        Source
c     ------------------------------------------------------------
   SDEF ERG=D1 POS=0 46 200
c
   SP1 -2 1.42
c
c
c ***************************************************************************
c
```

```
c    ***************************************************************************

c       Material Cards

c    ***************************************************************************
c
c   material-1,  Zinc-Sulfide
m1   16000        0.5
      30000        0.5
c
c   material-2,  Lithium-6
m2   03006        1.0
c
c   material-3,  poly
m3   06000.66c    0.33333
      01001.66c    0.66667
mt3   poly.60t
c ***************************************************************************
c
c    ***************************************************************************
c       Tally Cards
c    ***************************************************************************
c
nps 10000000
mode  n
f4:n 2
sd4 1.0
fm4 -1.0 2 105
c
c END FILE
```

VITA

Alex Okowita was born in Oakville, Ontario Canada, March 11, 1991. In 2001 he and his family moved to Charlotte North Carolina where he later graduated from Marvin Ridge High School in 2009. He then attended North Carolina State University and received his Bachelor of Science in Nuclear Engineering in 2013. After completing his bachelor's degree, he accepted a graduate research assistantship at the University of Tennessee in Knoxville under Dr. Jason Hayward. He worked at Oak Ridge National Laboratory under the steady eye of Dr. Alex Enders to conduct research on alternatives to Helium-3 under the Second Line of Defense Program. He completed his MS of Nuclear Engineering in December 2014.